



HAL
open science

Atomic Transport in Au-Ge Droplets: Brownian and Electromigration Dynamics

Frédéric Leroy, Ali El-Barraj, Pierre Müller, Fabien Cheynis, Stefano Curiotto

► **To cite this version:**

Frédéric Leroy, Ali El-Barraj, Pierre Müller, Fabien Cheynis, Stefano Curiotto. Atomic Transport in Au-Ge Droplets: Brownian and Electromigration Dynamics. *Physical Review Letters*, inPress. hal-02319455

HAL Id: hal-02319455

<https://hal.science/hal-02319455>

Submitted on 18 Oct 2019

HAL is a multi-disciplinary open access archive for the deposit and dissemination of scientific research documents, whether they are published or not. The documents may come from teaching and research institutions in France or abroad, or from public or private research centers.

L'archive ouverte pluridisciplinaire **HAL**, est destinée au dépôt et à la diffusion de documents scientifiques de niveau recherche, publiés ou non, émanant des établissements d'enseignement et de recherche français ou étrangers, des laboratoires publics ou privés.

Atomic transport in Au-Ge droplets: Brownian and electromigration dynamics

F. Leroy,^{1,*} A. El Barraï,¹ F. Cheynis,¹ P. Müller,¹ and S. Curiotto¹

¹*Aix Marseille Univ, CNRS, CINAM, Marseille, France*

(Dated: October 18, 2019)

The deposition of Au on Ge(111)- $\sqrt{3} \times \sqrt{3}$ -Au above the eutectic temperature results in the formation of AuGe liquid droplets that reach the liquidus composition by digging a hole in the Ge substrate. Combination of low energy electron microscopy and atomic force microscopy measurements show that AuGe droplets randomly migrate or electromigrate under an applied electric current dragging their underneath hole. The droplet motion is due to a mass transport phenomenon based on Ge dissolution at the droplet front and Ge crystallisation at its rear. At high temperature the mass transport is limited by attachment/detachment at the solid/liquid interface and the activation energy is 1.05 ± 0.3 eV. At low temperature the effective activation energy increases as function of the droplet radius. This behaviour is attributed to the nucleation of 2D layers at the faceted liquid-solid interface.

Diffusion, dissolution and crystallization phenomena occurring in alloys at the liquid-solid interface are crucial in the context of nanowires growth by the Vapor-Liquid-Solid mechanism or for the exploitation of low melting temperature solder materials [1–8]. To study these processes one approach consists in analyzing the fluctuation dynamics of the alloy or its response to a perturbation [9]. In that respect mass transport induced by an electric current [10–12] provides a unique opportunity to study atomic processes using the electric current as a control parameter [13–16]. For instance the motion of a liquid alloy droplet induced by a flowing electric current is intimately related to the atomic processes of diffusion and dissolution-crystallization at the liquid-substrate interface [17–19]. The dependence of the drift velocity with the current density, temperature, and droplet size provides key information on the kinetics and energetics of the system. If there is a key benefit to studying a directed motion rather than a random motion from a statistical analysis point of view, the counterpart is to know quantitatively the applied force. Experimental studies of the drift velocity of sub-micronic liquid metal entities, *e.g.* inclusions [20] in bulk or droplets [21 and 22] at surfaces subject to an electric current are still scarce despite numerous fundamental and practical implications [23 and 24]. Historically electromigration has been studied in solids and thin films [11, 12, 25–27]. It has been proposed that the driving force for atom migration arises from two sources: (i) the external electric field acts directly on the partially charged surface atoms and it is called direct force, (ii) the electric current carriers transfer a momentum to the atoms, this effect is called the wind force [28–30]. The experimental determination of the dominant process as well as the atomic mechanisms in liquid alloys appeals for dedicated studies [11 and 12].

This letter aims at addressing the atomic mechanisms of mass transport in Au-Ge alloy droplets on Ge(111). The bulk phase diagram shows a deep eutectic at Au₇₂Ge₂₈ (634 K). Therefore the deposition of Au on Ge(111) above the eutectic temperature results in the formation of liquid droplets. We show that these droplets incorporate Ge to reach the liquidus composition by dig-

ging a hole into the substrate. When an electric current is applied to the Ge(111) substrate, the droplets and their underlying holes move together in the direction of the electron flow. Therefore electromigration yields a Ge flux inside the droplet *via* dissolution at the front of the droplet and crystallization at the rear. We show that the droplet velocity depends linearly on the applied electric current and follows an Arrhenius law with two regimes: (i) a low temperature regime where the activation energy is droplet size-dependent pointing to a migration velocity limited by the nucleation of 2D layers at the solid-liquid interface. The step stiffness responsible for the nucleation barrier is about 4 meV.nm^{-1} at 700 K. (ii) A high temperature regime where the activation energy is size independent (1.05 ± 0.3 eV) and the migration mechanism is consistent with attachment-detachment kinetics at the liquid-solid interface. To disentangle the role of the electromigration force and the mass transport mechanisms in the droplet velocity, the droplets motion has also been studied in absence of electric current, *i.e.* in the brownian diffusion regime. It is shown that the electromigration force increases linearly with the droplet size indicating that the contact line between the substrate and the droplet plays a key role.

Ge(111) single crystals were cleaned by repeated cycles of ion bombardment (Ar⁺, E=1 keV, I=8 μ A) and annealing (1000 K). At last, the crystals were annealed close to the Ge melting point (1211 K) during a few seconds to obtain extended terraces at the surface [19] ($>10 \mu\text{m}^2$). The electric current was applied in the $\langle 110 \rangle$ directions. The sample temperature was adjusted independently from the electric current by using a complementary radiative W filament and an electron bombardment heating stage [31]. The temperature was measured with an Impac pyrometer (emissivity=0.56) that had been calibrated using the Ge(111)- $\sqrt{3} \times \sqrt{3}$ -Au to 1×1 -Au surface phase transition occurring at 913 K [32] and the eutectic melting point of Au-Ge droplets (634 K). Au was deposited by evaporation-condensation using a MBE-Komponenten effusion cell containing 5N Au shots. The nucleation and migration of Au-Ge droplets were

studied by low-energy electron microscopy (LEEM III, Elmitec GmbH) in bright field mode, with an electron-beam energy of 6.0 eV.

LEEM images in Fig. 1(a)-(b) show the motion of Au-Ge droplets on a Ge(111) single crystal under an applied electric current at 710 K. Au-Ge droplets nucleate preferentially at step edges but also on large terraces. Droplets that nucleate on terraces experience an oriented motion along the electron flow direction. Upon Au deposition, Au-Ge droplets grow in size and their velocity decreases. Finally when they reach a step edge, a step bunch or a phase boundary between two Ge(111)- $\sqrt{3} \times \sqrt{3}$ -Au domains they remain pinned. To rule out a potential artifact induced by thermomigration which may result from a residual thermal gradient on the sample, we have reversed the direction of the electric current. The migration direction is also reversed which confirms the dominant role of electromigration. Additionally LEEM images do not show any trail behind the migrating droplets. To fully characterize the nature of the surface left behind the motion of the droplets we have measured μ -LEED patterns in the trail of the droplets. The surface remains a Ge(111)- $\sqrt{3} \times \sqrt{3}$ -Au surface (spot size 150 μm radius, see inset Fig. 1(b) and Supplementary Materials S2). This confirms that the surface perfectly recovers its morphology (flat terrace) and crystalline structure after the passage of the droplet. Atomic Force Microscopy (AFM) images taken *ex situ* before and after selective etching of Au reveal that a shallow hole (≤ 2 nm depth, see Fig. 1(c)) is formed below each droplet inside the Ge(111) substrate [33 and 34] and is deeper as the droplet is larger. From these results we infer that the droplets and their underlying holes electromigrate both at once. The droplets migration is thus associated with Ge dissolution at the advancing front of the droplet and Ge crystallization at the rear.

In order to analyze in details the droplet electromigration mechanisms, we have studied the droplet velocity on atomically flat terraces as a function of droplet size, temperature and electric current density. The measurement of the droplet velocity v_D as a function of the electric current density at constant temperature points to a linear dependence without any current density threshold (see Supplemental Material S4). To estimate the electromigration velocity of a droplet v_D , a phenomenological approach is proposed based on Einstein relation, $v_D = \frac{\bar{D}}{k_B T} \bar{F}$, assuming an effective electromigration force \bar{F} acting on the droplet and a droplet diffusion coefficient \bar{D} . The diffusion coefficient is related to the atomic mechanism responsible for the mass transfers. We have evaluated the activation energy involved in the motion measuring the droplet velocity at constant electric current density ($5.6 \times 10^5 \text{ A m}^{-2}$) in the temperature range 650 K to 750 K. From an Arrhenius plot of $v_D \times k_B T$, we have found two regimes: (i) a high velocity regime (> 700 K) where the extracted activation energy E_a is size independent (1.05 ± 0.3 eV, Fig. 2-(b)). This experimental value is large if we consider that diffusion occurs

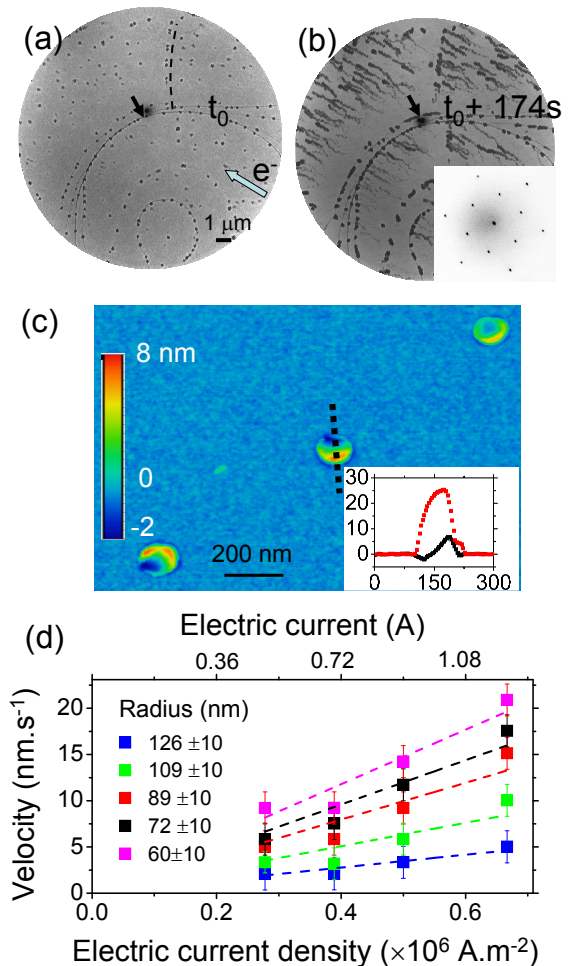


FIG. 1. (a) LEEM image of Au-Ge droplets on Ge(111)- $\sqrt{3} \times \sqrt{3}$ -Au (electric current density: $5.10^5 \text{ A}\cdot\text{m}^{-2}$, $T=710$ K, field of view: 15 μm). See Supplemental Material S1 at [URL will be inserted by publisher] for the complete movie. (b) Projection of 80 LEEM images (over 174 s) showing the trajectories of the Au-Ge droplets at the surface. Pinning of the droplets at step edges, step bunches and at phase boundary between two Ge(111)- $\sqrt{3} \times \sqrt{3}$ -Au domains are evidenced. The black arrow indicates a defect on the detector. Inset: μ -LEED pattern ($E=18$ eV) of the surface in the droplet trail (spot size 150 μm radius). See Supplemental Materials S2. (c) AFM image ($1.4 \times 0.9 \mu\text{m}^2$) of the surface after KI etching (see Supplemental Material S3 at [URL will be inserted by publisher] for the surface before etching). In inset is shown a height profile across a droplet (see dashed lines) before (red) and after etching (black). A hole is clearly visible and a rim of Ge is also put in evidence due to phase separation of Au and Ge when the sample is cooled at room temperature. Let us note that the substrate surface is also slightly roughened by KI.

in a liquid where typical energy barrier of 0.1 eV are reported [35]. It is also too large to be assigned to an enthalpy of fusion (~ 0.1 eV) arising from dissolution-crystallisation processes [36]. However such large activation energies have been measured for instance in the

case of the electromigration of Au inclusions into Si bulk [20] (0.92 eV) and may be associated with an interface attachment-detachment phenomena. We have also found (ii) a low velocity regime (< 700 K) where the activation energy increases with the droplet size to reach about 3 eV for 120 nm droplets radius (see Fig. 2-(b)). This result can not be assigned to usual mass transport phenomena based on diffusion mechanisms.

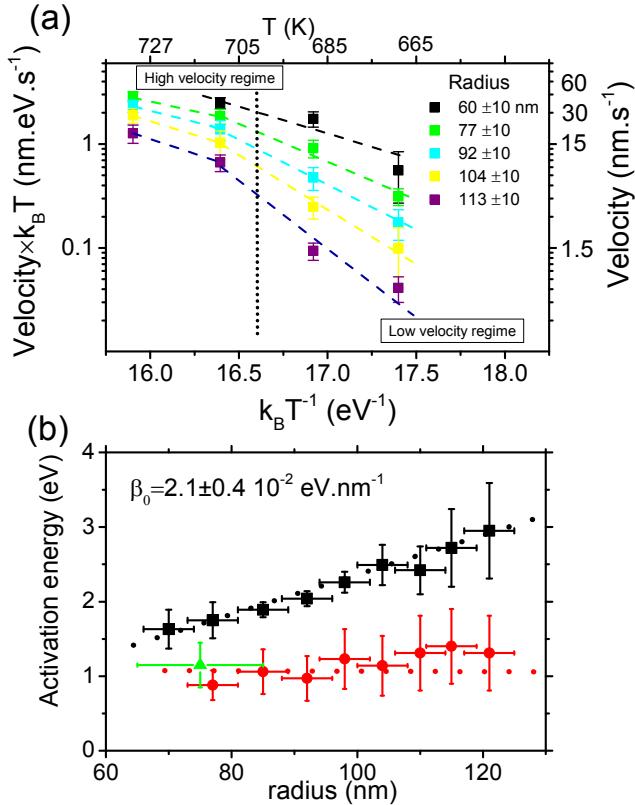


FIG. 2. (a) Arrhenius plot of the droplet velocity (averaged over 20 droplets per data point) v_D times $k_B T$ for different droplet radius and at constant electric current density. A high and low velocity regime can be distinguished (see dotted line of separation). (b) Plot of the activation energy versus the droplet radius in the low (black square) and high (red disk) velocity regimes. $\beta_0 = 2.1 \cdot 10^{-2} \text{ eV.nm}^{-1}$ is the slope of the activation energy versus droplet radius in the low velocity regime. Green triangle: activation energy for the droplet diffusion coefficient in the high temperature regime.

To lift the ambiguities on the mass transport mechanisms mediating the droplets migration, the respective role of the electromigration force and the droplet diffusion coefficient must be disentangled. To study the size dependence of the diffusion coefficient alone we have reduced the electric current to zero: the droplets are still mobile and move randomly at the surface. Therefore we have now access to the fluctuation part of the fluctuation-dissipation theorem. In Fig. 3-(b)-(c) are shown the trajectories of about 20 droplets on an atomically flat terrace ($\sim 10 \times 5 \mu\text{m}^2$) over ~ 500 seconds at $T = 677$ K. From

the mean square displacement of thousands of droplets as function of time t we can evaluate the diffusion coefficient $\bar{D} = \langle r^2 \rangle / 4t$. The diffusion coefficient decays as $\bar{D} \sim R^{-2.1 \pm 0.3}$ (R is the droplet radius) for temperatures higher than 693 K (Fig. 3-(d)). It drops much faster at lower temperature (*e.g.* 677 K). At high temperature the size dependence of the droplet diffusion coefficient \bar{D} can be analyzed using the random-walk theory or other formulations for uncorrelated atomic motion assuming different mass transport mechanisms (see Refs. [37–40] and Fig. 3-(a)). Following the line of thought of Refs. [37 and 41] we can describe the change in position of a droplet from individual atomic events independent from each other [42]. Let us consider for instance the kinetics of atom attachment-detachment (called also evaporation-condensation) at the liquid-solid interface. In this case the average time τ for an atomic jump scales inversely proportionally to the interface area $\tau \sim R^{-2}$ and the average droplet jump distance δ scales as $\delta \sim R^{-2}$. Therefore the diffusion coefficient of the droplet limited by attachment-detachment kinetics reads $\bar{D}_{AD} \sim \frac{\delta^2}{\tau} \sim R^{-2}$. A similar analysis gives $\bar{D}_V \sim R^{-3}$ when limited by volume diffusion and $\bar{D}_I \sim R^{-4}$ when limited by interface diffusion [43]. Therefore the high temperature behaviour of the diffusion coefficient $\bar{D} \sim R^{-2.1 \pm 0.3}$ can be assigned to a mass transport phenomenon limited by attachment-detachment kinetics at the solid-liquid interface. Moreover the Arrhenius plot of the diffusion coefficient provides the activation energy involved in this regime: $E_a = 1.15 \pm 0.3$ (green triangle in Fig. 2-(b)). This result is within the error bar the same as the activation energy for droplet electromigration at high temperature (> 700 K).

The low temperature regime is not compatible with attachment-detachment kinetics as the decay of the diffusion coefficient is too fast. This behaviour is observed much more precisely in the droplets velocity under electromigration (see Fig. 4) as a much better statistics can be achieved on a drift motion compared to a random motion. Indeed in the plot of the velocity versus droplet radius, two regimes can be analysed: (i) a high velocity regime where the velocity is a decreasing function of the droplet radius R and evolves as $v_D \sim R^{-1.3 \pm 0.3}$ and (ii) a low velocity regime at lower temperature (≤ 700 K) where it decreases exponentially (*e.g.* by a factor 30 from 100 to 150 nm radius at 687 K). We propose that the exponential decay of the low velocity regime can be assigned to the presence of facets at the liquid-solid interface responsible for interface-controlled processes such as nucleation of 2D layers. Such a mechanism has been theoretically investigated [37, 43–46] and observed for instance in 2D nanocrystal reshaping [47] or in the Brownian motion of 3D inclusions in bulk [48]. In presence of 2D layer nucleation it has been shown that a size dependent nucleation barrier $E_a = E_0 + \beta \cdot R$ for crystallisation or dissolution may occur [43, 45, and 48] where β is the step edge energy, R is the radius of the droplet and E_0 is a constant (volume diffusion energy barrier). The fit of the activa-

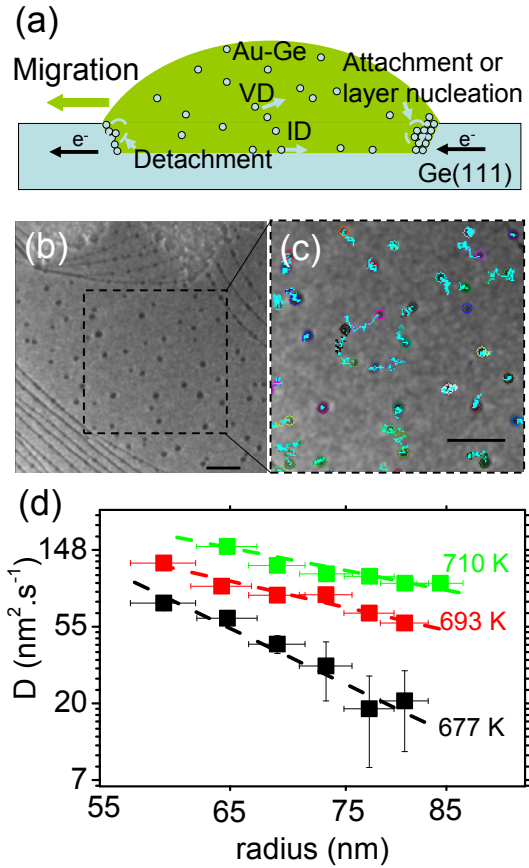


FIG. 3. (a) Scheme of possible mechanisms mediating the droplets migration: Interface Diffusion at the liquid solid interface (ID), Volume Diffusion (VD) and attachment-detachment or 2D layer nucleation at the interface (See Supplemental Material S5). (b) Bright field LEEM image of Au droplets during brownian migration ($T=677$ K). See Supplemental Material S6 at [URL will be inserted by publisher] for the complete movie (scale bar $1 \mu\text{m}$). (c) Close view of the trajectories (lines) of selected droplets during 562 s. (d) Log-Log plot of the droplet diffusion coefficient as function of the droplet radius. For $T=693$ K and 710 K, $\bar{D} \sim R^{-2.1 \pm 0.3}$. For $T=677$ K, \bar{D} decreases much faster indicating a change of diffusive regime.

tion energy at different temperatures shows that the step edge energy decreases from $4.4 \text{ meV} \cdot \text{nm}^{-1}$ at 669 K to $3.2 \text{ meV} \cdot \text{nm}^{-1}$ at 732 K (inset of fig. 4). Assuming a linear decrease of the step edge energy $\beta = \beta_0 \left(1 - \frac{T}{T_R}\right)$ we estimate that $\beta_0 = 19 \pm 4 \text{ meV} \cdot \text{nm}^{-1}$ and $T_R = 880 \pm 50$ K corresponding to the roughening transition temperature. This result is consistent with the estimate of $\beta_0 = 21 \pm 4 \text{ meV} \cdot \text{nm}^{-1}$ from the slope of the activation energy versus droplet radius (Fig. 2-(b)). It also matches the results of Radetic *et al.* [48] for Pb inclusion motion into a Al matrix providing $\beta_0 = 16 \text{ meV} \cdot \text{nm}^{-1}$ and $T_R = 820$ K.

Finally, it should be noted that the study of Brownian dynamics and that of the electromigration of droplets made it possible to independently measure the droplet

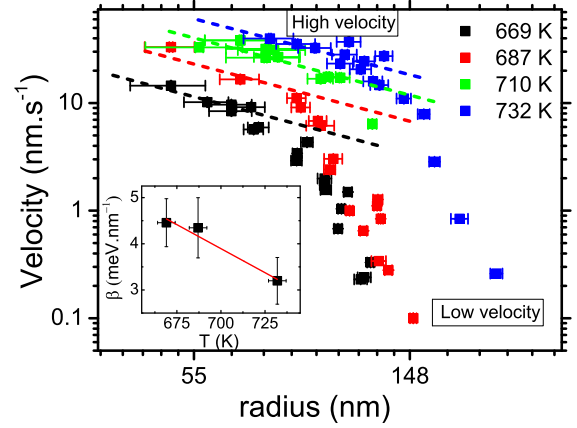


FIG. 4. Log-Log plot of the droplet velocity versus the droplet radius at different temperatures and at constant electric current density ($5.6 \times 10^5 \text{ Am}^{-2}$). In the high velocity regime $v_D \sim R^{-1}$ (dashed lines for each temperature), whereas the velocity decreases exponentially in the low velocity regime (low temperature and/or for large droplet sizes). Inset: Temperature evolution of the step edge stiffness β in the low temperature regime.

velocity and the droplet diffusion coefficient for different droplet sizes (in the high velocity regime). Therefore we have now access to the size dependence of the effective electromigration force $\bar{F} = kT \frac{v_D}{D} \sim R^{0.8 \pm 0.4}$ acting on the droplets. It scales approximately linearly with the droplet radius. This behaviour is consistent with a force acting at the droplet contact line resulting from deviations to the periodic crystal structure *e.g.* induced by the abrupt modification of the structure and electronic conductivity between the Ge single crystal and the AuGe liquid alloy.

In conclusion we have studied the brownian motion and the response to an electric current of Au-Ge droplets on extended terraces on Ge(111) above the eutectic temperature. The migration associates a hole that is formed into the substrate in order to reach the liquidus composition. We have explored two regimes: a high velocity regime (> 700 K) where according to size dependence of the droplet velocity and diffusion coefficient we show that the mass-transport mechanism is limited by attachment-detachment kinetics of atoms at the liquid solid interface and the driving force is acting at the contact line. This process is associated with an activation energy of 1.05 ± 0.3 eV. The low temperature regime is characterized by an activation energy of the droplet migration that is size dependent. This result is assigned to a mechanism of 2D nucleation of layers at the liquid solid interface. The estimated step edge energy decreases from 4.4 to $3.2 \text{ meV} \cdot \text{nm}^{-1}$ from 669 to 732 K and is expected to reach 0 at the roughening transition temperature $T_R = 880$ K. We believe that all these experimental measurements can be used as a tool to control the position of nanodroplets

on surfaces by means of an electric current and will be a new benchmark for further theoretical investigations on the dynamics of the droplets and associated mass transport phenomena.

This work has been supported by the ANR grants LOTUS (ANR-13-BS04-0004-02) and HOLOLEEM (ANR-15-CE09-0012).

* leroy@cinam.univ-mrs.fr

- ¹ H. Adhikari, A. F. Marshall, I. A. Goldthorpe, C. E. D. Chidsey, and P. C. McIntyre. *ACS Nano*, 1(5):415–422, 2007.
- ² A. D. Gamalski, J. Tersoff, R. Sharma, C. Ducati, and S. Hofmann. *Nano Lett.*, 10(8):2972–2976, 2010.
- ³ S. Kodambaka, J. Tersoff, M. C. Reuter, and F. M. Ross. *Science*, 316(5825):729–732, 2007.
- ⁴ E. A. Sutter and P. W. Sutter. *ACS Nano*, 4(8):4943–4947, 2010.
- ⁵ E. Sutter and P. Sutter. *Nanotechnology*, 22(29):295605, 2011.
- ⁶ P. W. Sutter and E. A. Sutter. *Nat. Mat.*, 6(5):363–366, 2007.
- ⁷ A. Sundar, P. Farzinpour, K. D. Gilroy, T. Tan, R. A. Hughes, and S. Neretina. *Small*, 10(16):3379–3388, 2014.
- ⁸ B. J. Kim, C. Y. Wen, J. Tersoff, M. C. Reuter, E. A. Stach, and F. M. Ross. *Nano Letters*, 12(11):5867–5872, 2012.
- ⁹ O. Pierre-Louis and T. L. Einstein. *Phys. Rev. B*, 62(20):13697–13706, 2000.
- ¹⁰ I. A. Blech and E. S. Meieran. *J. Appl. Phys.*, 40(2):485, 1969.
- ¹¹ P. S. Ho and T. Kwok. *Rep. Prog. Phys.*, 52(3):301–348, 1989.
- ¹² H. Yasunaga and A. Natori. *Surf. Sci. Rep.*, 15(6-7):205–280, 1992.
- ¹³ C. Tao, W. G. Cullen, and E. D. Williams. *Science*, 328(5979):736–740, 2010.
- ¹⁴ A. Kumar, D. Dasgupta, C. Dimitrakopoulos, and D. Maroudas. *Appl. Phys. Lett.*, 108(19), 2016.
- ¹⁵ A. Kumar, D. Dasgupta, and D. Maroudas. *Appl. Phys. Lett.*, 109(11), 2016.
- ¹⁶ Q. Liu, R. Zou, J. Wu, K. Xu, A. Lu, Y. Bando, D. Golberg, and J. Hu. *Nano Lett.*, 15(5):2809–2816, 2015.
- ¹⁷ S. Curiotto, F. Leroy, F. Cheynis, and P. Müller. *Surf. Sci.*, 632:1–8, 2015.
- ¹⁸ S. Curiotto, F. Leroy, F. Cheynis, and P. Müller. *Nano Lett.*, 15(7):4788–4792, 2015.
- ¹⁹ S. Curiotto, F. Leroy, F. Cheynis, and P. Müller. *Sci. Rep.*, 7, 2017.
- ²⁰ T. R. Anthony. *J. Appl. Phys.*, 51:6356, 1980.
- ²¹ T. Ichinokawa, H. Izumi, C. Haginoya, and H. Itoh. *Phys. Rev. B*, 47(15):9654–9657, 1993.
- ²² P. Kumar, J. Howarth, and I. Dutta. *J. Appl. Phys.*, 115(4):044915, 2014.
- ²³ Y. H. Lin, Y. C. Hu, C. M. Tsai, C. R. Kao, and K. N. Tu. *Acta Mater.*, 53(7):2029–2035, 2005.
- ²⁴ Y. C. Hu, Y. H. Lin, C. R. Kao, and K. N. Tu. *J. Mater. Res.*, 18(11):2544–2548, 2003.
- ²⁵ F. Leroy, P. Müller, J. J. Metois, and O. Pierre-Louis. *Phys. Rev. B*, 76(4), 2007.
- ²⁶ F. Leroy, D. Karashanova, M. Dufay, J. M. Debierre, T. Frisch, J. J. Metois, and P. Müller. *Surf. Sci.*, 603(3):507–512, 2009.
- ²⁷ Stefano Curiotto, Pierre Müller, Ali El-Barraj, Fabien Cheynis, Olivier Pierre-Louis, and Frederic Leroy. *Appl. Surf. Sci.*, 469:463–470, 2019.
- ²⁸ H. B. Huntington and A. R. Grone. *J. Phys. Chem. Solids*, 20:76, 1961.
- ²⁹ I. A. Blech. *J. Appl. Phys.*, 47(4):1203–1208, 1976.
- ³⁰ A. H. Verbruggen. *IBM J. Res. Dev.*, 32(1):93–98, 1988.
- ³¹ V. Usov, C. O. Coileain, and I. V. Shvets. *Phys. Rev. B*, 82(15):153301, 2010.
- ³² J.A. Giacomo. "A Low Energy Electron Microscopy Study of the Growth and Surface Dynamics of Ag/Ge(110) and Au/Ge(111)". PhD thesis, University of California, Davis, 2009.
- ³³ S. Hajjar, G. Garreau, L. Josien, J. L. Bubendorff, D. Berling, A. Mehdaoui, C. Pirri, T. Maroutian, C. Renard, D. Bouchier, M. Petit, A. Spiesser, M. T. Dau, L. Michez, V. Le Thanh, T. O. Mentès, M. A. Nino, and A. Locatelli. *Phys. Rev. B*, 84(12):125325, 2011.
- ³⁴ H. Zitouni, A. Mehdaoui, A. Spiesser, K. Driss Khodja, L. Josien, V. Le Thanh, and C. Pirri. *Acta Mat.*, 90:310–317, 2015.
- ³⁵ L. Battezzati and A. L. Greer. *Acta Metall.*, 37(7):1791–1802, 1989.
- ³⁶ H. Okamoto and T. B. Massalski. *Bulletin of Alloy Phase Diagrams*, 5(6):601–610, 1984.
- ³⁷ F. A. Nichols. *J. Nucl. Mat.*, 30:143–165, 1969.
- ³⁸ P. J. Goodhew and S. K. Tyler. *Proceedings of the royal society of London series A-Mathematical physical and engineering sciences*, 377(1769):151–&, 1981.
- ³⁹ LJ Perryman and PJ Goodhew. *Acta Metallurgica*, 36(10):2685–2692, 1988.
- ⁴⁰ P. A. Thiel, M. Shen, D.-J. Liu, and J. W. Evans. *J. Phys. Chem. C*, 113(13):5047–5067, 2009.
- ⁴¹ A Pimpinelli, J Villain, DE Wolf, JJ Metois, JC Heyraud, I Elkinani, and G Uimin. *Surface Science*, 295(1-2):143–153, 1993.
- ⁴² P. Jensen. *Rev. Mod. Phys.*, 71(5):1695–1735, 1999.
- ⁴³ P. Wynblatt and N.A. Gjostein. *Progress in Solid State Chemistry*, 9:21 – 58, 1975.
- ⁴⁴ N. Combe, P. Jensen, and A. Pimpinelli. *Phys. Rev. Lett.*, 85(1):110–113, 2000.
- ⁴⁵ W. W. Mullins and G. S. Rohrer. *J. Am. Ceram. Soc.*, 83(1):214–216, 2000.
- ⁴⁶ King C. Lai, Yong Han, Peter Spurgeon, Wenyu Huang, Patricia A. Thiel, Da-Jiang Liu, and James W. Evans. *Chemical Reviews*, 119(11):6670–6768, 2019.
- ⁴⁷ C. R. Stoldt, A. M. Cadilhe, C. J. Jenks, J.-M. Wen, J. W. Evans, and P. A. Thiel. *Phys. Rev. Lett.*, 81:2950–2953, 1998.
- ⁴⁸ T. Radetic, E. Johnson, D. L. Olmsted, Y. Yang, B. B. Laird, M. Asta, and U. Dahmen. *Acta Materiala*, 141:427–433, 2017.